Long Range Ultrasonic Inspection of Aircraft Wiring

Technique and hardware development

T. Parthipan, P. Jackson
Plant Integrity Ltd.
Granta Park, Great Abington
Cambridge, United Kingdom
Billy.parthipan@plantintegrity.com

A. Chong, M. Legg, A. Mohimi, V. Kappatos, C. Selcuk, T.H. Gan
Brunel University, Uxbridge, Middlesex, UB8 3PH, United Kingdom bic@brunel.ac.uk

S. Moustakidis, K. Hrissagis
Centre for Research & Technology Hellas, Greece
smoustakidis@gmail.com

***Abstract*— Inspecting complex aircraft wiring by means of ultrasonic non-destructive testing has been addressed. This paper discusses the progress on the development of software and hardware that enable a novel technique of Long Range Ultrasonic Testing – a subset of ultrasonic non-destructive testing to be implemented for the inspection of complex aircraft wires insulation. A representative aircraft wire was modelled to identify appropriate wave modes that can be utilized for the inspection. The modelling work was validated via laser interferometry. The sensor array was driven with the Teletest® pulser-receiver unit used in laboratory conditions to produce data for signal processing. Signal processing algorithms that combine baseline subtraction and anti-correlation algorithms were deployed to detect features as well as defects on cable insulation. Further work on validating the hardware, software and system integration is planned.**

Keywords*— Aircraft wires; Ultrasonic NDT; Pulser-receiver; Cable insulation

I. INTRODUCTION

Satisfactory performance of any aircraft depends to a great degree on the continuing reliability of its power system and its Fly-By-Wire control electronics. The integrity of cables and cable looms that provide connectivity to these systems is critical to flight safety. These cables are often insulated for the purpose of separating conductive materials that carry various levels of electrical voltages and current as well as to support fixing. The insulation of aircraft wiring degrade and/or get damaged over time due to extreme temperature, pressure and humidity levels that they are exposed to. Defects may also be introduced during maintenance due to human error. Common defects include the insulation developing cracks, becoming brittle and delaminating from the core of the wire. Consequently, this can potentially become a source of electrical unreliability or even a fire hazard. Cases in point were the losses of TWA Flight 800 in July 1996 [1] and Swissair Flight SR111 in September 1998 [2], in both of which there were approximately 230 fatalities. Experts investigating almost three decades of international aviation incidents between 1972 and 2000 found more than 400 wire related incidents. The Ageing Transport Systems Rulemaking Advisory Committee (ATSRAC) found 2281 individual discrepancies in 39 aircraft, 73 of which were deemed significant, 31% of these being concerned with wiring. It concluded that one in two of the aircraft studied had a serious wiring fault [3]. It is, therefore, essential to develop an inspection technique to accurately determine the health of electrical wiring, in particular to monitor/inspect the condition of the insulation during maintenance.

A. *Method of aircraft wire inspection*

Current NDT techniques such as Pulse Arrested Spark Discharge (PASD), Time Domain Reflectometry (TDR), Frequency Domain Reflectometry (FDR) and Infrared Thermography all possess some limitations in assessing the health of wire insulation. PASD requires the complete removal of insulation prior to inspection and for FDR and TDR methods, disconnection of one end of the wire is necessary to carry out the test. Full access of the entire length of the wire and line of sight is necessary in order to carry out thermographic inspection. In view of these limitations, current test methods can be time-consuming, inefficient and increase the risk of maintenance-induced failure [4].

II. LRUT OF AIRCRAFT WIRES

Long Range Ultrasonic Testing (LRUT) is a subset of ultrasonic Non-Destructive Testing mainly used for the inspection of oil & gas pipelines [5]. LRUT technique ensures that the material and its mechanical properties are not damaged or changed during inspection and it has the ability to detect defects for many meters in different shapes and type of structures such as pipes and plates. This technique enables the inspection to be carried out from a single point of access if required [6]. Implementing LRUT to inspect the aircraft wire could potentially avoid the cumbersome procedure of removing the whole segment of panel and consequently reduce the operation down time. In contrast to conventional ultrasonic NDT this novel technique utilizes the lower end of the ultrasonic spectrum in the frequency range of 20 kHz to 100 kHz in typical applications and extended to 1 MHz for specialized applications such as inspecting components with complex features [7]. The same LRUT principle applies for pipe or wire inspection; however the defect tolerance is generally smaller in size for aircraft than in pipe. To increase the probability of detection in aircraft wire, the system will sought to achieve a balance between the use of higher

frequency (i.e. sensitivity to small defect) and effect of signal attenuation (i.e. propagation length).

Potential of using LRUT technique for the inspection of wires had been demonstrated by [8] using Plant Integrity's pulser-receiver unit Teletest® system. However, a complete inspection system for inspection of aircraft wiring currently does not exist. Therefore, an inspection technique that can accurately detect defects in aircraft wiring insulations during maintenance is needed. Such a system will consist of a transducer array, automated signal processing and defect recognition software, and a handheld pulser-receiver unit, as illustrated in fig. 1.

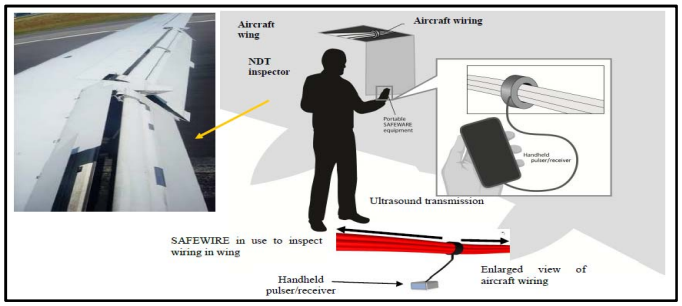

Fig. 1. Concept diagram showing the proposed LRUT aircraft wiring inspection system.

This paper presents the initial work in developing an overall system for inspection of aircraft wiring. To develop the technique, modelling of the aircraft wiring was performed for a representative wire to understand the ultrasonic guided wave (UGW) propagation. Dispersion curves were generated from the modelling work and validated using a 3D laser scanning vibrometer. Furthermore, an experimental procedure was devised to collect UGW signals in both pulse-echo and through-transmission mode. The data was used for development of signal processing and defect recognition routines. The concept and the initial progress of a hand-held pulser-receiver unit is also presented.

III. MODELLING

Finite Element Analysis (FEA) methods have been carried out to understand the concept of UGW propagation in insulated cables for defecting defects as well as features. The details of computing dispersion curves based on an eigenfrequencies analysis are described [4] [8]. This method revealed that at least three fundamental wave modes (longitudinal, torsional, and flexural) exist for a single core wire in the guided wave operating range of 10 kHz and 200 kHz. These techniques have also identified that the fundamental Torsional mode T(0,1) experiences minimal dispersion based on the specific dimensions and material properties used in the model. Likewise, for the longitudinal mode L(0,1), a similar non-dispersive mode with the highest phase velocity was noticed (approximately 3500 m/s). In contrast, the flexural mode exhibited dispersive characteristics. It is known that the longitudinal mode is generally less attenuative than other modes, and is more sensitive to transverse defects (due to their mode shapes). Therefore, it can be suggested that L(0,1) will be the most appropriate mode for this particular application of inspecting wires. The modelled dispersion curves were validated using a laser scanning vibrometer. An ultrasonic pulser/receiver was used to drive Macro-Fibre Composite (MFC) type P1 transducers [9] [10] using a chirp signal. The laser vibrometer was used to measure the M samples of the displacement of the wire with a sampling period of T. This was repeated for N locations separated by a distance r along a section of the wire. This displacement data was stored as a (NxM) sized matrix. A 2D-FFT was then applied to this matrix. This converted the matrix from the time-distance domain to the frequency-wavenumber domain. The resulting experimentally measured dispersion curves are plotted in fig. 2 (colored data) for the operating frequency range of up to 50 kHz, within which the best suited LRUT frequencies were identified. The modelled phase velocity v_{ph} dispersion curve results were converted to wave numbers using $k = \omega / v_{ph}$, where k and ω are the wave number and w is the angular frequency. These were then overlaid on the same figure (black dots). The dominant wave mode was L(0,1) at the frequency range of about 10 – 30 kHz. Reasonable agreement for both experimental measured and modelled dispersion curve was observed for this mode. The representative cable used in this experiment is shown as an insert in fig. 2.

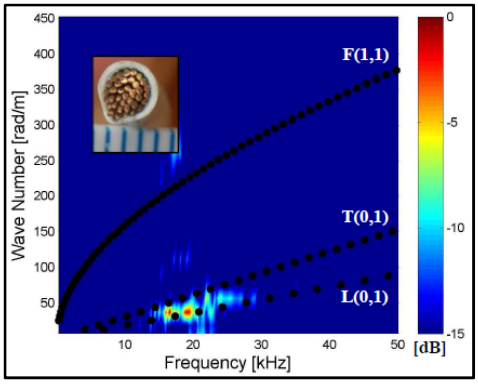

Fig. 2. Experimental dispersion curves with FEA modelling results overlaid (black dots) for the wire using the scanning laser vibrometer and MFC type P1 transducer.

IV. EXPERIMENTAL PROCEDURE

Experimental setup depicted in fig. 3 was used to perform UGW measurements on a 15m cable of type R015 in pulse echo and through transmission mode. For proof of concept, the chosen length of cable which represents a segment in the aircraft (i.e. wing or fuselage) is suspended using 4 poles with middle supporting poles at P1 and P2. The interval distance of the supporting poles are randomly placed at approximately 5 m separation to replicate the practical condition in the aircraft. Two MFC (longitudinal mode type) transducers were positioned at each end of the cable and driven by a Teletest® unit. A tone bursts (5-cycle Von-Hann windowed) was employed for transmit frequency range of 10 – 30 kHz with a step of 1 kHz. A total of 20 repetitions were performed for each frequency and the time domain signals were averaged to improve the signal to noise ratio (SNR). This procedure was initially performed with as received condition. These signals were later used as baseline signals for signal processing. Subsequently, well classified defects were introduced into the wire insulation shown in fig. 4. After the introduction of each defect, the data collection procedure was repeated.

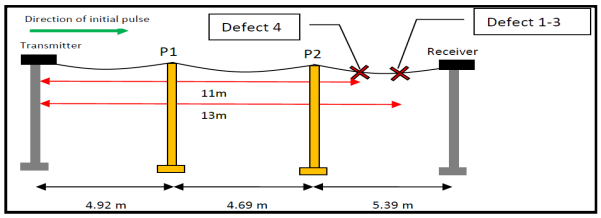

Fig. 3. Experimental setup

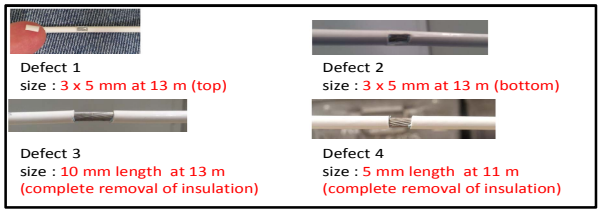

Fig. 4. Defects introduced to R015 cable

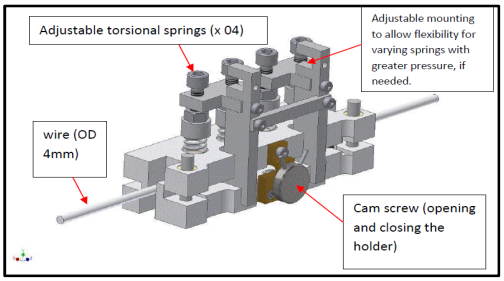

Fig. 5. Isomatric view of the prototyped sensor array

A sensor array has been prototyped to facilitate the technique development and initial trials. The isometric view of it is shown in fig. 5. 2 MFC transducers are fixed on the top and bottom jaws of the probe. It is equipped with a cam screw to ease inserting the test specimen and adjustable mechanism to allow variant of springs to be loaded for applying different pressure on the test specimen. This helps adjusting acoustic coupling effect between the transducers and the test specimen. This is a couplant free application.

V. SIGNAL PROCESSING

A variety of signal processing algorithms were implemented to accomplish the defect recognition and sizing task. A novel defect discrimination criterion was finally designed that combines the capabilities of well-known techniques that are given in the following:

Baseline subtraction as computed by:

$$\boldsymbol{x}'(n) = |\boldsymbol{x}(n) - \boldsymbol{m}(n)|, n = 0,1,2, \dots M \quad (1)$$

where $\boldsymbol{x} \in \mathbb{R}^M, M$ (scalar) the space dimensionality and $\boldsymbol{m} \in \mathbb{R}^M$ denotes the average baseline signal.

Cross-Correlation (CC) analysis [11] that was implemented using:

$$r_{W_t}(l) = \sum_{i=-\infty}^{\infty} \boldsymbol{x}_{W_t}(i)\boldsymbol{m}_{W_t}(i-l), \quad l = 0, \pm1, \pm2, \dots \quad (2)$$

Where $\boldsymbol{x}_{W_t}$ and $\boldsymbol{m}_{W_t}$ define window segments of **x** and **m** respectively**.** A cross-correlation signal $\boldsymbol{r}_{W_t}$ was computed at each time instant (t) of the acquired signals by i) extracting first the windowed segments $\boldsymbol{x}_{W_t}$ and $\boldsymbol{m}_{W_t}$ of a preselected size (L) and ii) computing the transform as given by (2). Finally, following a time dependent approach an anti-Cross-Correlation signal ($aCC \in \mathbb{R}^M$) was defined in this paper:

$$aCC(t) = 1 - max\{1 - \boldsymbol{r}_{W_t}\} \quad (3)$$

The computed $aCC(t) \in \mathbb{R}^M$ retains the same dimensionality with the acquired signals $\boldsymbol{x}$ and expresses the degree of similarity between a collected ultrasonic signal and the average baseline at the specific time instance t. If $aCC(t) \to 0$, the signals **x** and **m** are not correlated at the time instance t, whereas when $aCC(t) \to 1$ the signals **x** and **m** are highly correlated at the time instance t.

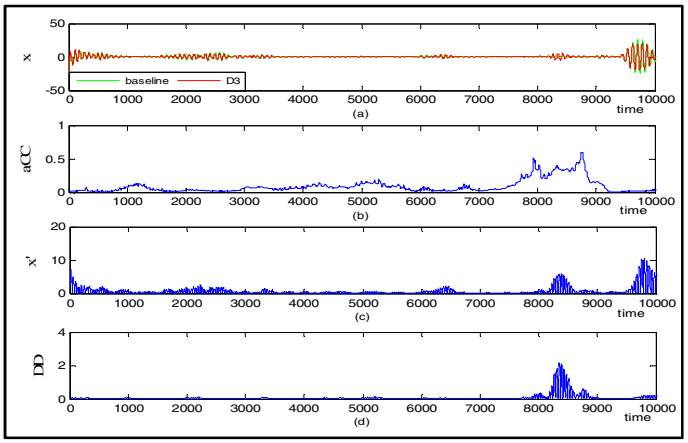

Fig. 6. a) Indicative acquired ultrasonic data from the baseline (green color) and the D3 defect class (red color), b) the computed Acc signal, c) the baseline subtracted output and d) the proposed hybrid DD signal.

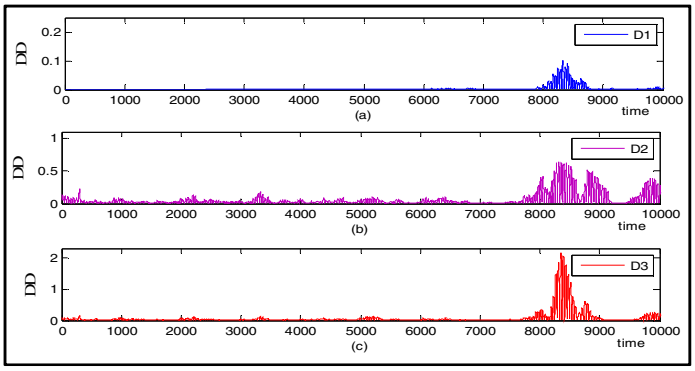

Fig. 7. Hybrid Defect Discrimination signals for the defect classes: a) D1, b) D2 and c)D3.

The aforementioned techniques and algorithms were implemented and validated on a real case scenario where a representative aircraft cable (Type R015) cable with a length of 15 m was utilized (fig.3 and fig.4). Artificial cuts of increasing size were created on the insulation of the cable and the efficiency of the aforementioned signal processing techniques was assessed in terms of their ability to improve the Signal-to-Noise Ratio (SNR). To optimise the signal generation process, an enriched and extensive data acquisition protocol was

adopted. A significant number of measurements (20) was conducted for each setup (for the defect free cable and the 5 defect categories). A series of tone bursts of gradually changing frequency was employed to generate signals with frequency sweeps in the frequency range 10 kHz – 30 kHz with a step of 1 kHz. The application of the signal processing techniques on this initial dataset contributed to extracting the first findings regarding the optimal frequency and the optimum signal generation process.

The aforementioned techniques (1)-(3) were applied on the acquired dataset and indicative results on a signal that belongs to D3 defect class are shown in Fig. 6. In Fig.6; a, the raw ultrasonic data is shown for both the baseline (with green color) and the D3 defect class (with red color). The generated aCC signal is shown in Fig. 6; b, whereas the result of baseline subtraction is given in Fig. 6; c.

As shown in Fig. 6; b, the aCC signal receives higher amplitudes in the area of [8000,9000] indicating that the signal $\boldsymbol{x}$ is less correlated with the average baseline in the specific time region. Moderate amplitudes are also received in the rest rime domain. In Fig. 6; c, where the result of the baseline subtraction is shown, high amplitudes are also received in the time region of [8000 ms, 9000 ms], whereas significantly high (or even higher) amplitudes are received in the rest signal.

To combine the discrimination capabilities of the aforementioned measures, a hybrid Defect Discrimination (DD) measure is proposed in this paper as given in the following:

$$\boldsymbol{DD}(n) = \boldsymbol{x}'(n) * \boldsymbol{aCC}(n), \qquad n = 0,1,2,\dots M \qquad (4)$$

Fig. 6; d, depicts the generated DD3 signal that improves considerably the Signal-to-Noise ratio (SNR) forming a valuable tool for defect detection, mapping and sizing. The hybrid DD signals DD1 and DD2 were also computed using indicative data from the D1 and D2 defect classes and accomplishing satisfying performances. As shown in Fig. 7, the proposed DD measure works efficiently in every defect size improving vastly the SNR of the collected data and therefore identifying even the smallest defects (D1).

The proposed in this paper hybrid DD measure forms a novel sophisticated tool for defect identifcation and localisation in aircraft wiring. In comparison with the commonly used baseline subtraction and cross-correlation analysis, the proposed technique accomplished considerable higher SNR being able to identify all the defect sizes (D1-D3) under investigation. The effectiveness of the proposed analysis suggest that the DD measure could be efficiently used, not only for wiring inspection but also for other large and complex infrastructures such as pipes, ship hull, bridges etc.

VI. Pulser Receiver Prototype

A battery powered handheld pulser-receiver is being developed to establish all the essential functions required to implement LRUT on aircraft wires. The main functionality of this unit is based on Plant Integrity Ltd.'s flagship product - the Teletest® system that is mainly used for inspecting oil & gas pipelines [10]. The handheld pulser-receiver under development however in contrast to Teletest® system is being developed with enhanced functionalities that allow medium frequency LRUT inspection (10 kHz to 500 kHz) at higher excitation voltages of up to 400 VAC while maintaining the portability to size 200 mm x 100 mm x 50 mm and weight 1 kg.

Work published by [8] and [4] evident that LRUT inspection of conductors (uninsulated) require higher excitation frequencies in the 200 kHz range for achieving acceptable resolution. In contrast, the modelling and experimental results described above indicate that there is higher attenuation present in cable insulation, limiting the inspection range when higher frequency LRUT is applied on insulated cables. This means lower excitation frequency in the 20 kHz range is sufficient for satisfying the primary scope of this project of inspecting cable insulation. This framework 7 project known as Safewire is looking at extending the inspection range to beyond 10 m from the datum point where the transmit transducer is placed. Decision had been made by the consortium at the conceptual stage of this project to develop the hardware to enable medium frequency, higher voltage excitation LRUT for the optimum usage of the hardware by allowing inspection on conductors (not a primary scope of this project) as well as insulation (primary scope). Exciting piezoelectric transducers at high voltage produce higher ultrasonic energy, which help overcome the attenuation in general. Other ways of increasing the transmit power are also going to be implemented by increasing the number of cycles present in the excitation signal envelop. Increasing number of transducers may not be possible because of the physical size constraints imposed by the small cable diameter and the complexity of bundles.

TABLE I. Proposed hardware specification

Description	Proposed specification
Number of transmit and Receive channels	2 - Transmit; 2 - Receive
Transmit frequency	10 kHz - 500 kHz
Transmit voltage	300 VAC
Receive circuit resolution	12 bits
Receive sampling rate	5 Mhz
Battery specification	15 VDC Nom.; 5.3 Ah
Display	7" touch screen LCD
Dimension	250 mm x 200 mm x 60 mm
Weight	1 kg

The proposed hardware specification of the pulser-receiver unit is presented in table 1. This unit is being designed as a duel channel unit (2 x transmit and 2 x receive) for allowing backward cancellation during transmission and reception. Receive circuit resolution has been selected as 12 bits for achieving -72 dB noise floor which has been proved adequate for this application by the Teletest® application. The receive RF signals are sampled at the maximum of 5 MHz. A 15 V (Nom.) Li-Ion battery of capacity 5.3 Ah has been specified for the extended operational lifetime. The weight and the physical dimensions have been specified as 1 kg and 250 mm x 200 mm x 60 mm for optimum portability.

A. Hardware functionality

The diagram indicating the basic functional units of the handheld pulser-receive is shown in fig. 8. The unit will have 2 transmit channels and 2 receive channels (optional 4) for allowing backward cancellation during transmission and reception. A Matlab based Graphical User Interface (GUI) was

developed to facilitate input parameters into the inspection system. The application specific software is built-in with all relevant Dynamic Link Libraries (DLLs) that are required to interface with the Xilinx Spartan 3A DSP FPGA based control electronics from the GUI. The control electronics hardware is governed by micro-blaze microprocessor intellectual property IP integrated in the FPGA.

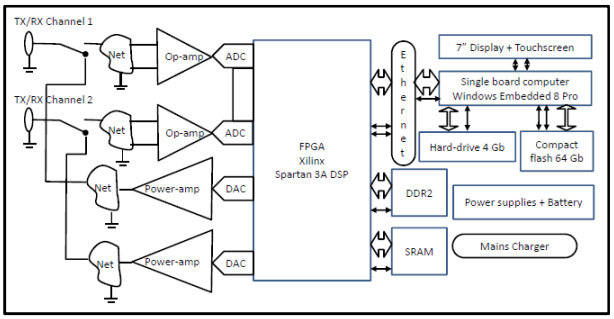

Fig. 8. Simplified architecture of the pulser-receiver

The transmit channels support an array of piezoelectric transducers. Each transmit channel is capable of exciting a capacitive load of maximum value 5 nF, with the maximum of 400 VAC at excitation frequency 500 kHz. The simplified schematic of this circuit, the description of its topology and the need for a high voltage power supply that satisfy the Power Supply Rejection Ratio (PSRR -110 dB) of the designed circuit are documented by the authors in [6] and is not repeated in this paper. The excitation signal profile is generated and downloaded into the Block RAM of the FPGA by the application software based on user input parameters during configuration phase. This is subsequently fed into the 16 bit DACs which consequently drive the piezoelectric load via the power amplifiers. A +/-200 VDC power supply is implemented in the design that converts the battery voltage of 15V into +/-200 VDC for supporting the power amplifiers.

Receive channels utilize commercial ADCs and are capable of digitizing 12 bits and can be configured via the GUI to sample data at clock speeds from 1 MHz to 5 MHz in 1 MHz steps. A bank of asynchronous SRAMs is used to store and accumulate the digitized data during data collection before transferred to the DDR2 bank. This final data is then uploaded into the onboard memory of the Single Board Computer (SBC) via 10/100 Ethernet which then be signal processed by the novel signal processing algorithms discussed in section IV for displaying data in the form of A-Scan and/or pass/fail message.

B. Firmware

The FPGA implements all relevant logic for configuring the hardware to provide raw data capture in a pulse-echo or pitch-catch mode (through-transmission) and test/calibrate hardware in monitor mode. The functionalities are being implemented in the FPGA using VHDL and the main functionalities implemented are as follows: Top level sequencing, controller for the asynchronous SRAM to enable store and accumulation of captured data, ADC interface, DAC interface, power supply unit controls, transmit/receive switching, error handling and test functions. Xilinx IP cores for DDR2 controller, Ethernet 10/100, register interface for communication with micro-blaze microprocessor using its peripheral bus are some of the other main functionalities included in the FPGA. In a typical application the FPGA is loaded on power up from an on-board flash memory. New firmware bit stream can be reloaded in to this memory via LAN for in situ reloading purposes. The system also allows the FPGA to be loaded directly from a JTAG without overwriting the flash memory.

C. Software

The software implemented forms an integral part of the design. Its development followed layered approach from the low level drivers to the high level graphical user interface for simplifying the routine calls that are required for the configuration of the hardware, executing data collection, data readout for signal processing and displaying results. Low level drivers were implemented using C library routines and the graphical user interface was developed using Matlab. Fig. 9 shows the layered design implemented.

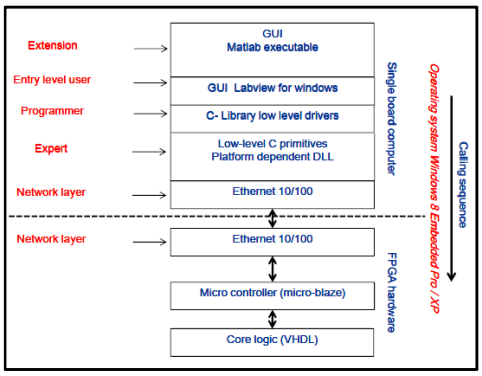

Fig. 9. Layered software architecture implemented

VII. HARDWARE STATUS

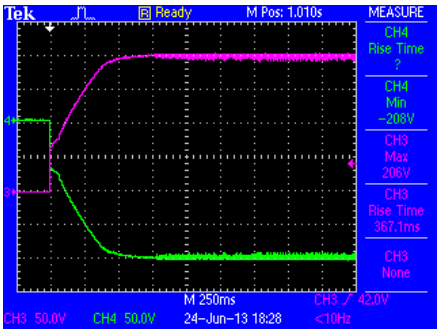

Fig. 10. High voltage power supply rails raming up to +/-200V

Hardware has been produced and is being tested at present. Duel channel transmit circuit that is capable of exciting 5 nF capacitive load at 400 VAC for the excitation frequencies ranging from 10 kHz to 500 kHz has been realized and tested successfully. Fig. 10 shows the high voltage power supply rails (CH3: +200V; CH4: -200V) ramping up and regulated at +/-200V DC on demand. These are the power supply rails to the power amplifier transmit circuits that excite the piezoelectric transducers. Fig. 11 shows the output of the transmit circuit (CH1: transmit channel 1, CH3: transmit channel 2) delivering 400 VAC; 20 kHz excitation signal to a piezoelectric transducer array; each channel driving a capacitive load of

value 5 nF. CH4 shows the input signal to the power amplifier. The amplifier is configured to x50 gain.

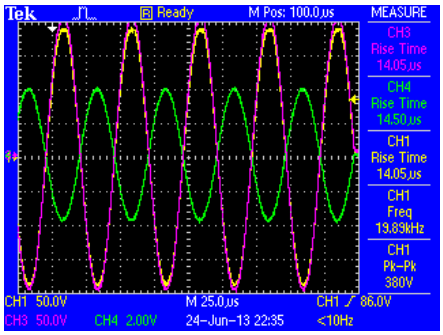

Fig. 11. Excitation signal exciting 5 nF capacitive load at 400V, 20 kHz

Fig. 12, shows an excitation signal of voltage 400V and frequency 500 kHz (CH1) exciting the same load. CH3 and CH4 shows the high voltage power supply rails regulated at +/- 200V during the excitation.

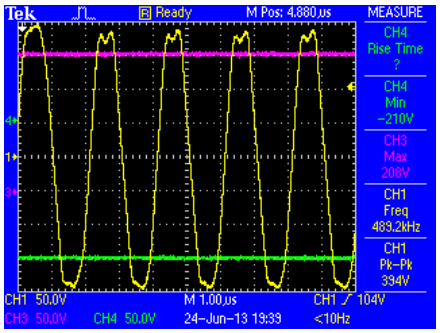

Fig. 12. Excitation signal exciting 5 nF capacitive load at 400 V, 500 kHz

The rest of the hardware and a conceptual design of the packaged hardware are presented in fig. 13; left and right respectively.

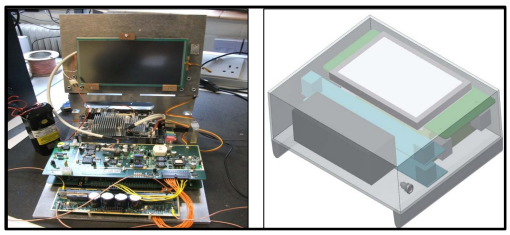

Fig. 13. Hardware developed (left); Conceptual drawing of the unit (right)

A. *Field trials*

The field trials are expected to be carried out at the End User facilities. The trials will either be carried out on a C-130 airplane, depending on their availability at the time of field trials, or alternatively on a section of a C-130 wing.

B. *Applications outside Safewire*

Opportunities outside the inspection of aircraft wiring is possible with this system such as inspecting railway signal wiring, control wiring in large ships, wiring in large building, etc.

VIII. CONCLUSION

Challenges of detecting defects on cable insulations has been met by the employment of L(0,1) mode UWG in the lower end of the LRUT operating frequency. Signal processing method hybrid-defect-discrimination-metric algorithm that combines baseline subtraction and anti-cross-correlation signal processing methods allowed defects to be identified effectively and reliably. Further work on the enhancement of the signal processing method and the hardware is planned.

IX. ACKNOWLEDGEMENT

The research leading to these results has received funding from the European Union's Seventh Framework Programme managed by REA-Research Executive Agency http://ec.europa.eu/research/rea ([FP7/2007-2013]) for the project entitled “Long range ultrasonic inspection of aircraft wiring” – SAFEWIRE, under grant agreement no [313357] , FP7-SME-2012-1 (http://www.safewire.eu). SAFEWIRE is collaboration between the following organisations: HORTEC, PLANT INTEGRITY LIMITED, ASSIST, POLKOM BADANIA SP ZOO, ATARD, MARSHALL ADG, BRUNEL UNIVERSITY and CERTH.

X. REFFERNCES

[1] NTSB, "Aircraft Accident Report - Trans Wold Airlines Flight 800," 17 July 1996. [Online]. Available: http://www.ntsb.gov/doclib/reports/2000/AAR0003.pdf. [Accessed 24 11 2013].

[2] TSB-Canada, "Transportation Safety Board of Canada," July 2001. [Online]. Available: http://www.tsb.gc.ca/eng/medias-media/fiches-facts/A98H0003/sum_a98h0003.asp. [Accessed 24 11 2013].

[3] ATSRAC, "Non-Invasive Inspection - Part 1," 2002.

[4] Y. Gharaibeh, "EngD Thesis: The application of guided waves for Non-Destructive examination of complex structures," Brunel University, London, 2010.

[5] P. Mudge and P. Catton, "Monitoring of Engineering Assets using Ultrasonic Guided Waves," in *Proceeding of the 9th European Conference on Non-Destructive Testing*, Berlin, 2006.

[6] T. Parthipan, P. Mudge, R. Nilavalan and W. Balachandran, "Design and analysis of ultrasonic NDT instrumentation through system modelling," *International Journal of Modern Engineering,* vol. 12, no. 1, pp. 88 - 97, Fall/Winter 2011.

[7] G. A. Haig and P. Stavrou, "Defect detection for aircraft components: An approach using ultrasonic guided waves and neural networks," in *NDT2012*, 2012.

[8] Y. Gharaibeh, S. Soua, G. Edwards, P. Mudge and W. Balachandran, "Modelling Guided Waves in Complex Structures Part 2 - Wire Bundles with and wirhout insulation," in *BINDT Conference of NDT*, Blackpool, 2010.

[9] F. Sch□pfer, F. Binder, A. W□stehoff and T. Schuster , "Accurate determination of dispersion curves of guided waves in plates by applying the matrix pencil method to laser vibrometer measurement data," *CEAS Aeronautical Journal,* pp. 1-8, 2012.

[10] D. Alleyne and P. Cawley, "A two-dimensional Fourier transform method for the measurement of propagating multimode signals," *The Journal of the Acoustical Society of America,* vol. 89, p. 1159, 1991.

[11] S. J. Orfanidis, Optimum Signal Processing: An Introduction. 2nd Edition., New Jersey: Englewood Cliffs: Prentice Hall, 1996.